

High pressure effect on structure, electronic structure and thermoelectric properties of MoS₂

Huaihong Guo,¹ Teng Yang,^{1,*} Peng Tao,¹ Yong Wang,¹ and Zhidong Zhang¹

¹*Shenyang National Laboratory for Materials Science,
Institute of Metal Research and International Centre for Materials Physics,
Chinese Academy of Sciences, 72 Wenhua Road, Shenyang 110016, PRC*

(Dated: August 30, 2012)

We systematically study the effect of high pressure on structure, electronic structure and thermoelectric properties of 2H-MoS₂, based on first-principles density functional calculations and the Boltzmann transport theory. Under pressure, cross-plane lattice size reduces much faster than in-plane one due to weak van der Waals interaction and it gets more difficult to shrink the size as external pressure goes higher than 20 GPa, which agrees with experimental observation. A conversion from van der Waals bonding to covalent-like is found from charge density calculation. Concurrently, the dependence of band structure on pressure shows that a transition from semiconductor to metal occurs at 30 GPa. Band features close to Fermi level are discussed, such as narrow band from Γ to A and pressure-induced decrease of the band dispersion, which are advantageous for high values of thermopower. Our transport calculations also find that pressure-enhanced electrical conductivities, as well as high values of thermopower (up to a few hundred $\mu\text{V/K}$), lead to significant values of thermoelectric figure of merit (above 0.10 for high pressure and even up to 0.65 at 30 GPa) over a wide temperature range. Our study supplies a new practical route to improve the thermoelectric performance of MoS₂ and of other transition metal dichalcogenides by applying hydrostatic pressure.

PACS numbers: 31.15.A- 73.50.Lw, 72.80.Ga,

I. INTRODUCTION

MoS₂, a typical member of transition-metal chalcogenide family, consists of alternating sandwiched sub-layers bonded by van-der-Waals (VDW) interaction. This weak inter-layer interaction, which has rendered it a good solid lubricant¹, proves also essential in determining manifold novel properties, such as Raman frequency^{2,3}, band-gap type (direct, indirect) and band-gap size^{4,5} changing with number of stacking layers. Besides the method of layer stacking, one also resorts to applying external pressure (stress) to further tune the inter-layer interaction⁶. To our best knowledge, pressure-induced effect on the VDW interaction has not been theoretically investigated.

VDW interaction gives rise to some intriguing properties on one hand, to a poor electrical transport properties⁷⁻¹⁰ on the other. MoS₂ and other transition metal dichalcogenide materials were reported to have very pronounced value of thermopower, but poor electrical conductivity⁷⁻¹⁰, in result of a negligibly small value of dimensionless thermoelectric figure of merit ($ZT \sim 0.006$ at the optimal doping and working temperature)¹¹. To improve upon its electrical conductivity for a better value of ZT , pressure/stress may be employed and expected to suppress VDW bonding or to convert it to covalent or metallic type. Encouragingly, similar studies have already been performed on the single layer. Stress-induced enhancement of electron mobility in MoS₂ single layer has been demonstrated in experiment¹² for a promising nano-electronic device. Both compressive¹³ and tensile strain¹⁴ in a single layer give rise to a reduced band gap from first-principles calculations. A

semiconductor-metal transition was obtained for a compressive strain of about 15% for single-layer MoS₂¹⁴. So far, there have been no reports on pressure effect on bulk electrical properties. Moreover, how pressure affects the electronic structure and if it can ultimately improve its thermoelectric properties have never been investigated.

In this work, combining first-principles density functional calculations with semiclassical Boltzmann transport theory(BTT), we study the structure, electronic structure and thermoelectric transport properties of MoS₂ under hydrostatic pressure. Our calculation shows a vanishing anisotropy of structural change at around 20 GPa, agreeing with the experimental data⁶. We also find a concurrent conversion from VDW interaction to weak covalent-like type. A further compression induces a stronger covalent bonding and a semiconductor-metal transition at about 30 GPa. This transition improves greatly the inter-layer electrical conductivity but still keeps a large value of thermopower ($\sim 200\mu\text{V/K}$), therefore giving rise to much enhanced thermoelectric transport properties. Values of figure of merit (ZT) as high as 0.15 for in-plane direction and as 0.65 along cross-plane direction are obtainable in a wide range of temperature (from 100 K to 700 K). Our study demonstrates that applying high hydrostatic pressure can be an effective way to improve the thermoelectric performance of MoS₂ and of other transition-metal dichalcogenides.

II. METHODOLOGY

MoS₂ has $P6_3/mmc$ space group symmetry and consists of a hexagonal plane of Mo atoms sandwiched by

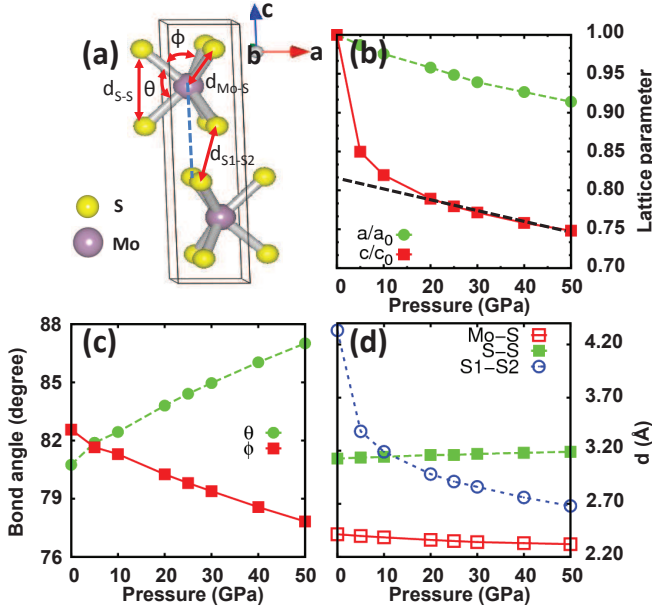


FIG. 1. (Color online) (a) Illustration of unit cell of MoS₂ and definition of the bond length $d_{\text{Mo-S}}$, $d_{\text{S-S}}$, $d_{\text{S1-S2}}$ and angles θ and ϕ . The dependence on hydrostatic pressure of (b) lattice parameters a/a_0 and c/c_0 , (c) bond angles, (d) bond lengths. A black dashed line in (b) is used to guide the eye.

two hexagonal planes of S atoms. The unit cell contains two alternating layers with an AB stacking along c axis, as illustrated in Fig. 1.

Band structure of MoS₂ is calculated by using the general potential linearized augmented plane-wave (LAPW) method as implemented in the WIEN2K package¹⁵. The electronic exchange-correlation is described within the generalized gradient approximation (GGA) of Perdew-Burke-Ernzerhof (PBE) flavor¹⁶, which has been proved also efficient in dealing with the weak inter-layer interaction within MoS₂⁴. We use 5000 k points in the full Brillouin zone (BZ) to achieve a self-consistency accuracy better than 1 meV/atom. The Engel-Vosko GGA (EV-GGA) formalism¹⁷ is applied to calculate the band gap more accurately.

Transport properties were calculated based on the Boltzmann transport theory applied to the band structure. The integration is done within the BOLTZTRAP transport code¹⁸. A very dense mesh with up to 18000 k points in the BZ is used. The electron scattering time is assumed to be independent of energy due to its good description of thermopower $S(T)$ in a number of thermoelectric materials^{19–21}.

We fully relaxed the unit cell volume, shape and internal atomic coordinates under each hydrostatic pressure till the internal atomic force is less than 10^{-2} eV/Å. We consider the external hydrostatic pressure no larger than 50 GPa where no occurrence of structural phase transition has been observed experimentally⁶ and structure remains to have P_{63}/mmc space group symmetry.

III. RESULTS AND DISCUSSION

We first studied pressure effect on structure of MoS₂ and understand the discontinuous structural variation observed in experiment⁶. Below 20 GPa, reduction of lattice parameters with pressure are anisotropic along in-plane and cross-plane directions, c/c_0 shrinks much faster than a/a_0 . This anisotropy vanishes above 20 GPa, which agrees with experiment by R. Aksoy et. al.⁶ and we analyzed by looking into internal structural parameters including bond angles and bond lengths, as shown in Fig. 1(c,d). In Fig. 1(c), opposite trends occur between the pressure dependencies of S-Mo-S bond angle θ and ϕ . Along with in-plane Mo-S and S-S bonds remaining relatively rigid in Fig. 1(d), pressure reduces the inter-layer distance via rotating Mo-S bond but very slightly. More importantly, $d_{\text{S1-S2}}$ (the distance between adjacent sulfur layers), presented in Fig. 1(d), shrinks abruptly with pressure especially below 20 GPa. This indicates a substantial pressure induced change of inter-layer interaction.

To see what happens to inter-layer interaction upon pressure, we studied total charge densities under hydrostatic pressures ranging from 0 to 50 GPa in Fig. 2. Along with $d_{\text{S1-S2}}$ decreasing with pressure, VDW interaction seems to disappear, a weak covalent-like bond starts to form at 20 GPa and grows stronger. Compared to no charge distribution between two neighboring layers as marked in dashed white frame at 0 GPa in Fig. 2(a), electron charge becomes more and more converged between the atoms S₁ and S₂ as illustrated from Fig. 2(b) to (d). Obviously, VDW type bonding is converted to covalent bonding due to pressure.

The change of inter-layer interaction will naturally lead to dependence of band structure on pressure from which we did find a transition from semiconductor to metal. Fig. 3 gives the calculated band structure evolving with pressure from 0 to 50 GPa. Fermi energies of semicon-

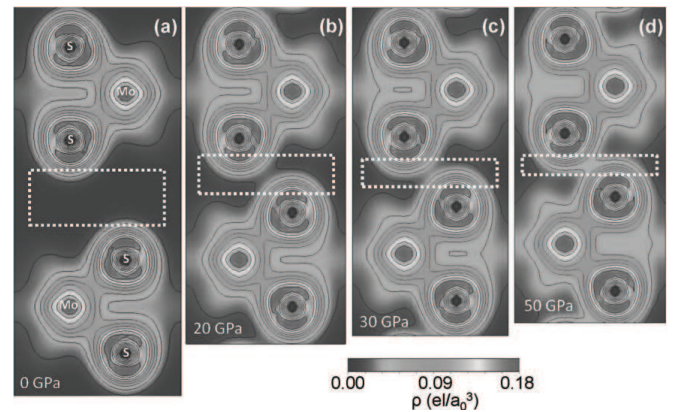


FIG. 2. (Color online) Total charge density ρ of MoS₂ (a) at 0 GPa, (b) at 20 GPa, (c) at 30 GPa and (d) at 50 GPa, seen from (110) cutting plane. A gradual change of bonding from (a) van-der-Waals type to (d) covalent-like type is seen.

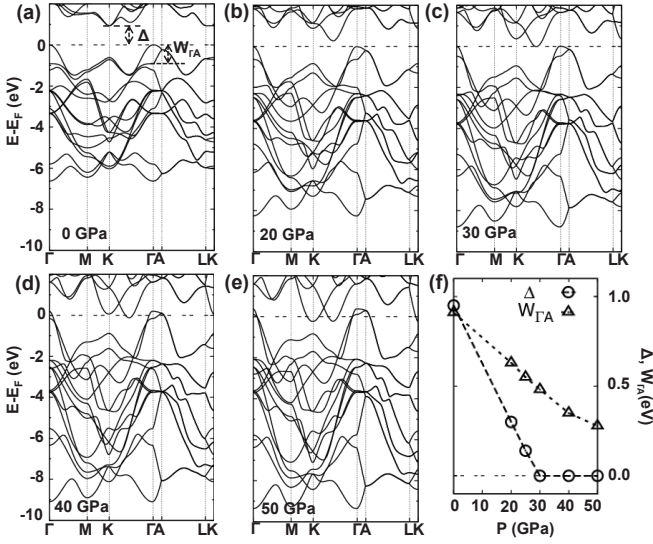


FIG. 3. (a-e) EV-GGA electronic band structure of MoS₂ under different hydrostatic pressures. The size of band gap decreases gradually with external pressure till 30 GPa where a semiconductor to metal transition occurs, as illustrated in (f). Band gaps Δ and $W_{\Gamma A}$ are defined in (a).

ductors are set at valence band maximum (VBM). The behavior of band gap is shown from (a) to (e) and summarized in (f). Indirect band gap Δ is initially between VBM at Γ point and conduction band minimum (CBM) at K point at zero pressure, but applying pressure will cause the CBM to shift to between K and Γ points. Δ drops linearly with pressure till a semiconductor-metal transition occurs at 30 GPa. This only takes a compressive strain of 7%, in contrast to 15% in single layer¹⁴. It seems much easier for the bulk material than the single layer to close the band gap Δ by applying pressure, due to the existing inter-layer interaction.

It is worth noting that, an increase of band dispersion with pressure is observed, except for two bands near Fermi level between Γ and A points. These two bands are actually zone-folded from one band as unit cell has one sub-layer. For convenience, both bands are treated as one with band width $W_{\Gamma A}$, as defined in Fig. 3(a). $W_{\Gamma A}$ decreases from 1 eV (at 0 GPa) via 0.50 eV (at 30 GPa) to 0.25 eV (at 50 GPa), an approximate linear dependence of $W_{\Gamma A}$ on external pressure is seen from Fig. 3(f).

To understand the counterintuitive behavior of the band dispersion decreasing with pressure, we look into its electronic state at 30 GPa in Fig. 4. In the energy range close to Fermi level, we are only concerned with Mo-d and S-p orbitals (Fig. 4(a,c)), since they play predominant roles in forming conduction channels for both in-plane and cross-plane directions. In Fig. 4(b,d), the two cross-plane bands with the anomalous width $W_{\Gamma A}$ are due to hybridization of Mo- d_{z^2} and S- p_z orbitals. The valence band at Γ point has a Γ_4^- symmetry^{5,22,23}, and the band below has a dominating contribution of

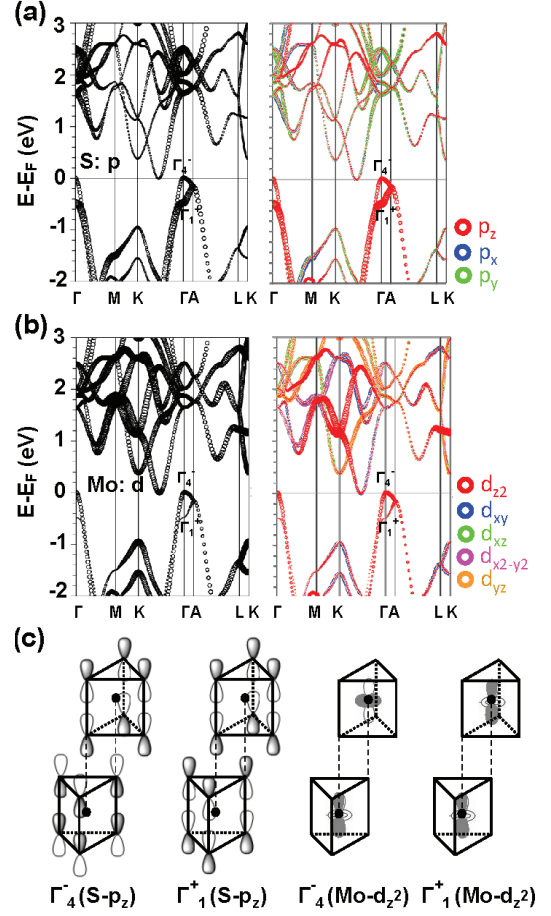


FIG. 4. (Color online) Electronic band character at hydrostatic pressure of 30 GPa. The electronic states close to E_F is mainly from (a) Mo-d and (c) S-p orbitals. (b) S- p_z and (d) Mo- d_{z^2} play major roles for cross-plane conduction channel. Possible combinations of S- p_z and Mo- d_{z^2} orbitals in MoS₂ unit cell is illustrated in (e) with symmetry labels used for the irreducible representations of the P6₃/mmc space group (Ref. 22).

S- p_z orbitals with Γ_1^+ symmetry^{22,24} at Γ point. The symmetries of possible combinations of Mo- d_{z^2} and S- p_z orbitals are illustrated in Fig. 4(e). We found the valence band have S- p_z anti-bonding characteristic. In this sense, the shrinkage of inter-layer distance d_{S1-S2} with pressure suggests a stronger anti-bonding state and therefore a narrower band dispersion near E_F from Γ to A. It also indicates that the band with Γ_1^+ symmetry at Γ point contributes to bonding. As pressure increases from 30 GPa, the Fermi level shifts down from VBM by unpopulating the antibonding state between Γ and A and is expected to strengthen the bonding state between sub-layers, which agrees with the charge density dependence on pressure as depicted in Fig. 2.

From the band structures shown above, we can also extract some useful information on the electrical conductivity. In Fig. 3(c-e), we found Fermi velocity (v_F) and effective mass (m^*) respectively increases and decreases

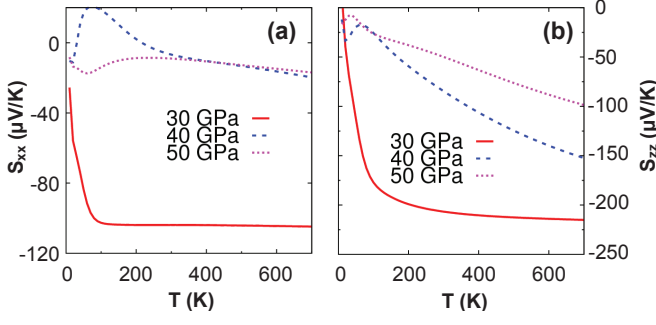


FIG. 5. (Color online) Dependence of thermopower on the temperature under different hydrostatic pressures along (a) in-plane direction and (b) cross-plane direction, respectively.

with pressure. Calculated electronic densities of states (DOSs) (not shown here) close to Fermi level at 30, 40 and 50 GPa are 0.07, 0.30 and 0.60 electrons/eV/u.c., respectively. Under thermal excitation within a range of interest (e.g., 700 K, equivalent to 0.06 eV of energy), DOSs translate to carrier concentrations n of approximately 5×10^{26} , 2×10^{26} and $5 \times 10^{25} \text{ m}^{-3}$ for 30, 40 and 50 GPa, respectively. The boost of carrier concentration (n) by pressure, together with increased v_F and reduced m^* , suggest pressure-enhanced electrical conductivity.

Also information on thermopower can be extracted from the band structures. According to the Mott relation²⁵, thermopower depends crucially on the derivative of logarithmic electrical conductivity over energy close to Fermi level^{26,27}, namely, $S \sim \frac{\partial \ln \sigma}{\partial E} \big|_{E=E_F}$. Based upon this, at the transitional pressure, a high value of thermopower is anticipated for both in-plane and cross-plane directions. Moreover, the anomalous bands upon pressure get more localized due to inter-layer anti-bonding states existing and its band edges have a big chance to touch Fermi level. It is therefore more advantageous for having high values of thermopower along cross-plane direction. Meanwhile, the carrier concentration ($n \sim 10^{26} \text{ m}^{-3}$) obtained above is lower by orders of magnitude than that in good metals ($n \sim 10^{28} \text{ m}^{-3}$). The lower level of carrier concentration, the higher value of S ²⁸. Much higher values of thermopower will be expected in our metallic MoS_2 with pressure above 30 GPa than that in good metals, which are actually confirmed by our following calculations.

We discussed qualitatively how pressure affects thermopower and electrical conductivity from band structure. Now we turn to semi-classical Boltzmann transport theory to quantify thermoelectric parameters of MoS_2 .

Firstly, we calculated thermopower as function of pressure and temperature. In Fig. 5, high values of thermopower were indeed obtained from 30 to 50 GPa. Especially, over 100 $\mu\text{V/K}$ in the plane and more than 200 $\mu\text{V/K}$ along c-axis are achievable over a wide temperature range in the region close to 30 GPa. Also from Fig. 5, a strong anisotropy of thermopower between two per-

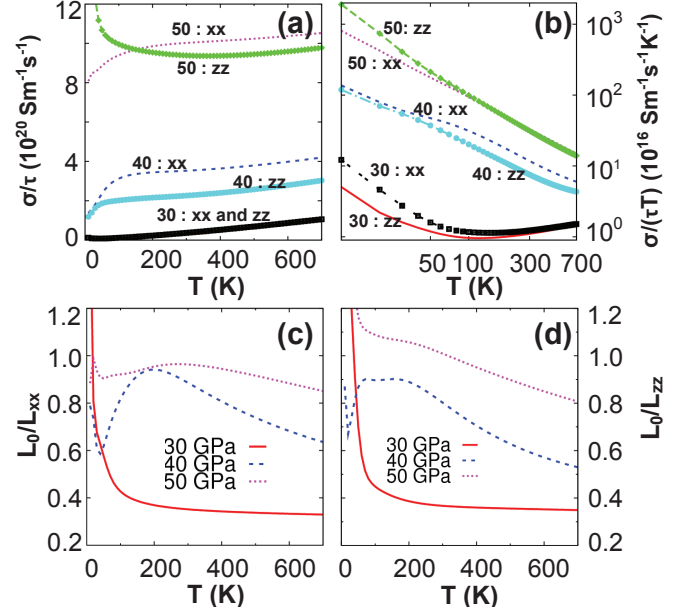


FIG. 6. (Color online) (a) The ratio of electrical conductivity σ over electronic relaxation time τ and (b) $\frac{\sigma}{\tau T}$ as function of pressure and temperature. (50 : xx) used in (a,b) means (pressure : direction). The ratio of Lorenz number L_0 over $\frac{\kappa_e}{\sigma T}$ along (c) in-plane and (d) cross-plane direction under various pressures above 30 GPa is given to test if the Wiedemann-Franz law fits here.

pendicular directions appears when pressure increases. The in-plane thermopower drops substantially while the cross-plane thermopower goes down fairly modestly.

In Fig. 6(a), we then show calculated σ/τ as function of pressure and temperature. σ/τ increases with external pressure, so does σ if τ is approximately pressure independent. To see how temperature dependence of σ but without available experimental τ , we assume electrons are mainly scattered by phonons at high temperature and electronic relaxation time $\tau \sim T^{-1}$ is used^{26,29}. Hence $\sigma/(\tau T)$ as function of temperature can give information on temperature dependence of σ . We show $\sigma/(\tau T)$ versus temperature in Fig. 6(b). Typical metallic behavior is seen by an inverse power law relation between $\sigma/(\tau T)$ and temperature, except for at 30 GPa where a slight deviation from the inverse power law is observed and suggests its conductive properties different from typical metals.

Electronic thermal conductivity κ_e/τ was also calculated but not given here. Alternatively, we put κ_e and σ in the background of the Wiedemann-Franz law and draw a ratio of Lorenz number ($L_0 = 2.8 \times 10^{-8} \text{ W}\Omega/\text{K}^2$) over L ($= \frac{\kappa_e}{\sigma T}$) as function of temperature and pressure in Fig. 6(c,d). The ratio shows a better obedience of the Wiedemann-Franz law as pressure increases from 30 to 50 GPa, L_0/L approaches unity as pressure gets to 50 GPa. In contrast to anisotropic thermopower S for two perpendicular directions, isotropic behaviors are found of dependence of L on temperature and pressure between

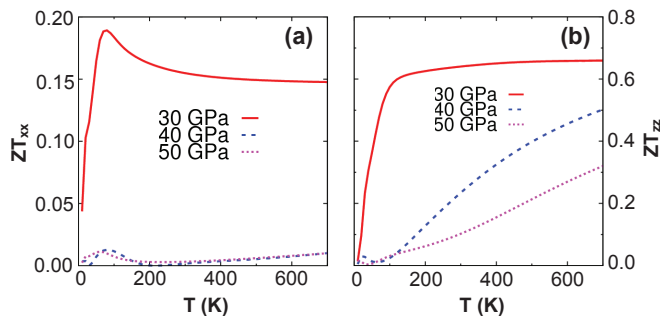


FIG. 7. (Color online) Temperature and pressure dependence of figure of merit ZT of conductive MoS_2 along (a) in-plane and (b) cross-plane directions. The cross-plane is more preferable for practical thermoelectric application.

in-plane and cross-plane directions.

As is known, dimensionless thermoelectric figure of merit ZT is defined as $\frac{S^2\sigma T}{\kappa_e + \kappa_l}$ (or $\frac{S^2}{L + \eta}$), with κ_l as the thermal conductivity of lattice part and $\eta = \frac{\kappa_l}{\sigma T}$. Assuming κ_l is insignificant to κ_e for metallic state³⁰ above 30 GPa, we show calculated ZT value in Fig. 7. Value of ZT can reach 0.15 along in-plane direction and 0.65 along c axis over a wide range of temperature at 30 GPa. As pressure increases, the values of ZT decrease. The in-plane ZT drops very abruptly, while the cross-plane ZT still has value higher than 0.10 over a wide range of pressure, suggesting a proper range of pressure is essential to optimize the thermoelectric properties.

IV. CONCLUSION

In summary, we systematically study the structure, electronic structure and thermoelectric properties of 2H- MoS_2 under hydrostatic pressure, based on the Boltzmann transport theory and first-principles density functional calculations. We find it becomes more difficult to reduce size along the cross-plane direction under pressure higher than 20 GPa, because of a crossover from weak inter-layer VDW interaction to covalent-like bonding. A quantitative agreement between our calculations and experimental data is reached. A semiconductor-metal transition is found to occur at 30 GPa and a much smaller compressive strain in bulk material than in single layer is needed for closing the band gap. Along with the pressured-enhanced electrical conductivity, we also obtained very large values of the thermopower (up to a few hundred $\mu\text{V/K}$ from 100 to 700 K) and ascribed it to some anomalous band features. Above all, good values of figure of merit are found. Besides, an anisotropy of ZT value is found to exist between two perpendicular directions. The cross-plane direction is more preferable. Its ZT value under pressure can be obtained as big as 0.10 and even up to 0.65 at 30 GPa over a wide temperature range. Our study supplies a new practical route to improve the thermoelectric performance of MoS_2 and of other transition metal dichalcogenides by applying hydrostatic pressure.

ACKNOWLEDGMENTS

This work was supported by the NSFC under Grant No. 11004201, 50831006 and the National Basic Research Program (No. 2012CB933103). T.Y. acknowledges the IMR SYNL-T.S. Kê Research Grant for support.

* E-mail: yangteng@imr.ac.cn

¹ J. M. Martin, C. Donnet, T. Le Mogne, and T. Epicier, Phys. Rev. B **48**, 10583 (1993).

² C. Lee, H. Yan, L. E. Brus, T. F. Heinz, J. Hone, and S. Ryu, ACS Nano **4**, 2695 (2010).

³ A. Molina-Sánchez and L. Wirtz, Phys. Rev. B **84**, 155413 (2011).

⁴ S. W. Han, H. Kwon, S. K. Kim, S. Ryu, W. S. Yun, D. H. Kim, J. H. Hwang, J.-S. Kang, J. Baik, H. J. Shin, et al., Phys. Rev. B **84**, 045409 (2011).

⁵ A. Klein, S. Tiefenbacher, V. Eyert, C. Pettenkofer, and W. Jaegermann, Phys. Rev. B **64**, 205416 (2001).

⁶ R. Aksoy, Y. Ma, E. Selvi, M. Chyu, A. Ertas, and W. A., J. Phys. Chem. Solids **67**, 1914 (2006).

⁷ R. Mansfield and S. A. Salam., Proc. Phys. Soc. B **66**, 377 (1953).

⁸ S. G. Thakurta and A. Dutta., J. Phys. Chem. Solids. **44**, 407 (1983).

⁹ M. Agarwal and L. Talele., Sol. State Comm. **59**, 549 (1986).

¹⁰ J.-Y. Kim, S. M. Choi, W.-S. Seo, and W.-S. Cho, Bull. Korean Chem. Soc. **31**, 3225 (2010).

¹¹ H. H. Guo, T. Yang, Y. Wang, P. Tao, and Z. D. Zhang, submitted (2012).

¹² B. Radisavljevic, A. Radenovic, J. Brivio, V. Giacometti, and A. Kis, Nature Nanotechnology **6**, 147 (2011).

¹³ W. S. Yun, S. W. Han, S. C. Hong, I. G. Kim, and J. D. Lee, Phys. Rev. B **85**, 033305 (2012).

¹⁴ E. Scalise, M. Houssa, G. Pourtois, V. Afanas'ev, and A. Stesmans, Nano Res. **5**, 43 (2012).

¹⁵ P. Blaha, K. Schwarz, G. K. H. Madsen, D. Kvasnicka, and J. Luitz, *WIEN2k, An Augmented Plane Wave Plus Local Orbitals Program for Calculating Crystal Properties* (Vienna University of Technology, 2001).

¹⁶ J. P. Perdew, K. Burke, and M. Ernzerhof, Phys. Rev. Lett. **77**, 3865 (1996).

¹⁷ E. Engel and S. H. Vosko, Phys. Rev. B **47**, 13164 (1993).

¹⁸ G. K. H. Madsen, K. Schwarz, P. Blaha, and D. J. Singh, Phys. Rev. B **68**, 125212 (2003).

- ¹⁹ K. P. Ong, D. J. Singh, and P. Wu, Phys. Rev. B **83**, 115110 (2011).
- ²⁰ D. Parker, M.-H. Du, and D. J. Singh, Phys. Rev. B **83**, 245111 (2011).
- ²¹ L. Zhang and D. J. Singh, Phys. Rev. B **80**, 075117 (2009).
- ²² L. F. Mattheiss, Phys. Rev. B **8**, 3719 (1973).
- ²³ Γ_4^- symmetry: antisymmetric electronic states from two MoS₂ sub-layers with respect to inversion, symmetric with respect to horizontal mirror plane within one sub-layer.
- ²⁴ Γ_1^+ symmetry: symmetric electronic states from two MoS₂ sub-layers with respect to inversion, symmetric with respect to horizontal mirror plane within one sub-layer.
- ²⁵ M. Cutler and N. F. Mott, Phys. Rev. **181**, 1336 (1969).
- ²⁶ J. M. Ziman, *Principles of the theory of solids*, 2nd Ed. (Cambridge University Press, 1995).
- ²⁷ K. P. Ong, D. J. Singh, and P. Wu, Phys. Rev. Lett. **104**, 176601 (2010).
- ²⁸ G. D. Mahan, *Solid State Physics*, vol. 51, ed. by H. Ehrenreich and F. Spaepen (Academic Press, 1998).
- ²⁹ J. M. Ziman, *Electrons and phonons* (Clarendon Press, 2001).
- ³⁰ The lattice contribution to thermal conductivity κ_l is insignificant here than electronic κ_e , due to following reasons. (1) At low temperature, electronic thermal conductivity κ_e dominates in the metals. (2) At high temperature, κ_e is insensitive to temperature under the circumstance of $\tau \sim T^{-1}$, while κ_l decreases with temperature, as experiments suggested¹⁰. It makes κ_e even more significant than κ_l at high temperture. (3) It would reduce our estimation of ZT by only one half if κ_l were comparable to κ_e .